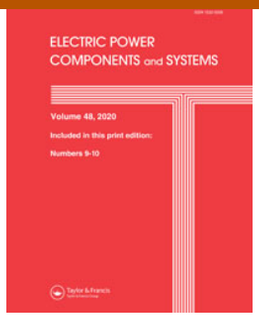

Electric Power Components and Systems

ISSN: (Print) (Online) Journal homepage: https://www.tandfonline.com/loi/uemp20

A Novel Method to Optimize Permanent Magnet Assisted Synchronous Reluctance Machines

Thushanthan Mohanarajah , Mahmood Nagrial , Jamal Rizk & Ali Hellany

To cite this article: Thushanthan Mohanarajah , Mahmood Nagrial , Jamal Rizk & Ali Hellany (2020) A Novel Method to Optimize Permanent Magnet Assisted Synchronous Reluctance Machines, Electric Power Components and Systems, 48:9-10, 933-943, DOI: 10.1080/15325008.2020.1821837

To link to this article: https://doi.org/10.1080/15325008.2020.1821837

Electric Power Components and Systems, 48(9-10): 933–943, 2020

ISSN: 1532-5008 print / 1532-5016 online
DOI: 10.1080/15325008.2020.1821837

A Novel Method to Optimize Permanent Magnet Assisted Synchronous Reluctance Machines

Thushanthan Mohanarajah, Mahmood Nagrial, Jamal Rizk, and Ali Hellany
School of Computing, Engineering, and Mathematics, Western Sydney University, Sydney, Australia

CONTENTS

Abstract—This paper presents the characteristics of permanent magnets in a synchronous reluctance machine by employing analytical and finite element methods. Four possible designs are studied and their characteristics are compared against a base synchronous reluctance machine with linear barriers to reveal machine characteristics. Then, the paper proposes a novel optimization topology to optimize permanent magnet synchronous reluctance machine as a single object for better machine performance. An explicit investigation is conducted to reveal the operational behavior of the machine such as torque, power factor and torque ripples with various machine parameters and compares them with the base design. The study reveals that permanent magnet synchronous reluctance machine can be optimized to have significantly high-power factor and torque with acceptable torque ripples.

1. INTRODUCTION

International standards, government policies and local legislation around the world require efficient electrical equipment to reduce energy consumption and reduce carbon emission on the environment. It emphasizes the search for alternative machines that can provide better efficiency with rugged and reliable operation. Consequently, new machines are developed and synchronous reluctance machine (SynRM) is one of them [1]. And another one is PM assisted synchronous reluctance machines (PMSynRM), the added optimum volume of PM in this machine provides even better machine performance compared with SynRM but with less PMs to conventional PM machines [1–7]. SynRM is known for its high torque density in a compact size. On the other hand, it is also renowned for poor power factor (pf) and torque ripples [8, 9]. The PMSynRM has a combination of reluctance (dominant) and magnetic torque components with improved pf and torque ripples in a compact size compared with its counterparts [1, 10–15].

PMSynRM exhibits better machine characteristics in all aspects with wide constant power speed range (CPSR)

Keywords: synchronous reluctance machine, PM assisted synchronous reluctance machines, machine design, reluctance machines, design optimization

Received 30 August 2019; accepted 23 August 2020

Address correspondence to Thushanthan Mohanarajah, School of Computing, Engineering, and Mathematics, Western Sydney University, Sydney, Australia. E-mail: thushanthan_engit@yahoo.com

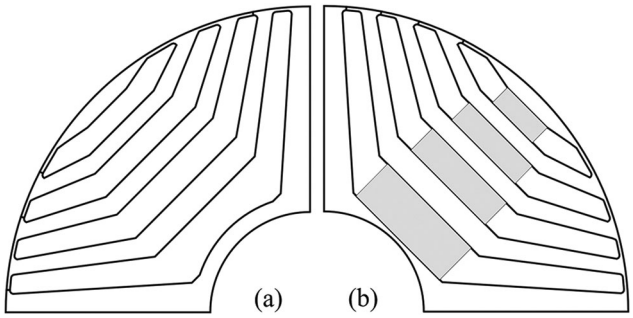

FIGURE 1. SynRM and PMSynRM share same rotor (a) Synchronous reluctance machine (b) PM assisted synchronous reluctance machine.

[12, 15, 16]. An optimized rotor flux guides, PM size and proper placement can compensate the drawback of synchronous reluctance motors [17, 18]. In PMSynRM, the PMs are introduced to obstruct the Q axis flux to saturate the rotor ribs. Consequently, the Q axis inductance is minimized, and the machine saliency is enhanced. Figure 1(a, b) shows a reluctance machine and PMSynRM where PMs are inserted into the linear flux guides along Q – axis. The introduction of PM and saturation of the ribs reduce the stator current i_q . The added magnetic flux in the D – axis enhances the back emf which results in increased power factor of the machine [16, 19].

SynRM has just reluctance torque component produced by its anisotropy structure whether transversally laminated or axially laminated. PM synchronous machines (surface mounted or interior mounted) has just a magnetic torque component due to the PM flux-linkage. Unlike those two types of machines, PMSynRM has both reluctance and magnetic torques where the reluctance torque is the principal component of the two. Therefore, this machine does not need high-grade PM, and ferrite magnets can be used to achieve the additional magnetic torque.

On the other hand, if the machine is not properly optimized, it can have higher cogging torque. It also produces a high voltage at the terminal end due to the larger constant power speed range (CPSR) as the controlled flux-linkage at this region may be less than the PM induced flux-linkage [9, 15]. The drawbacks of PMSynRM can be overcome by adequate optimization of the anisotropy model and properly placing PMs. An optimized machine with magnets and minimizing the PM quantity can have improved machine performance in comparison to its counterpart interior and surface permanent magnet machines [7]. Numerus research papers have been published in optimization of SynRM and optimization of PMs, but optimization of PMSynRM as a whole object is never attempted due to the complication [10, 20–26]. Optimization process automatically vary the flux barrier dimensions. The challenge in optimizing PMSynRM as a whole object is that when the flux barriers changes its location and shape, the added PMs should follow the flux barriers. It is achieved by a novel method in this paper.

A test synchronous reluctance machine with four linear barriers, as shown in Figure 1(a) is used for initial investigation, and an optimized SynRM is studied for further PM optimization. The machine performance parameters, i.e. torque density, power factor, torque ripples and efficiency are explicitly studied and optimized.

2. ANALYSIS OF SYNRM

The saliency of SynRM is defined by the ratio of D & Q inductance or differences in the inductances Eq. (1). The primary characteristic and design parameter is the machine saliency ratio in the case of SynRM that governs torque density Eqs. (2) and (3) as well as pf [27]. However, high saliency in SynRM requires exceptional anisotropy with controlled saturation. By ignoring the rotor saturation and stator slotting effects, the torque of SynRM can be simplified as shown in Eq. (2) where p is the number of poles, L_d & L_q and i_q & i_d are inductances, currents in direct, and quadrature axes respectively. The torque of the SynRM machine is directly related to the variances in D & Q axes inductances Eq. (4).

On the other hand, the resultant flux-linkage of PMSynRM is impacted by added magnets. While the D axis PM flux-linkage can be ignored, the Q axis one is the resultant of stator and PM induced in opposite directions, as shown in Eq. (3). Therefore, the torque of PMSynRM can be derived by the simplified version as given in Eq. (4). The first term is reluctance torque, and the second one is PM torque. The PM torque depends on various characteristics such as PM grade, placement, and optimization of PM. However, this type of machine can have numerous possible designs between the two-torque combinations, as shown in Figure 2.

$$\xi = L_d / L_q \tag{1}$$

$$T_{SynRM} = \frac{3}{2}\ p\ [(L_d - L_q) i_q i_d] \tag{2}$$

$$\lambda_d^{PM} = L_d i_d\ \ \&\ \ \lambda_q^{PM} = L_q i_q - \ \lambda_{PM} \tag{3}$$

$$T = \frac{3}{2} p\ \left[(L_d - L_q) i_q i_d + \ \lambda_{PM} i_q\right] \tag{4}$$

The saliency ratio (ξ) differs between each type of salient pole machines. The variation in saliency (ξ) is

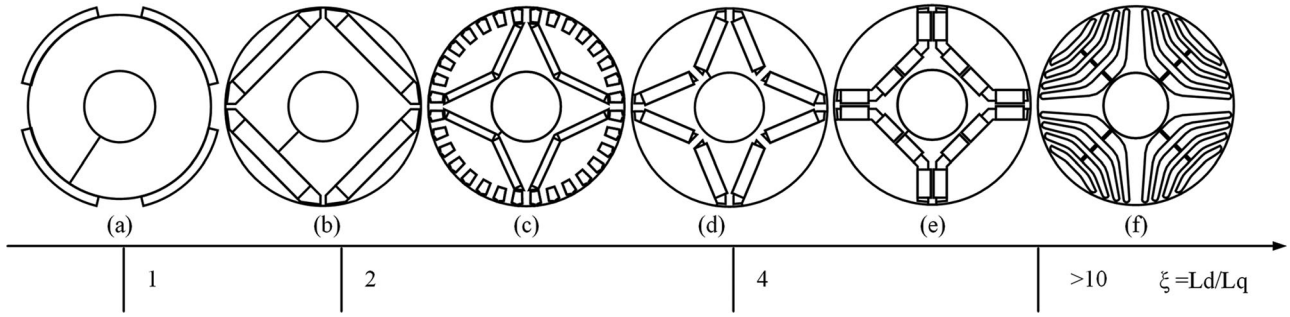

FIGURE 2. Saliency comparison of PM synchronous and synchronous reluctance machines.

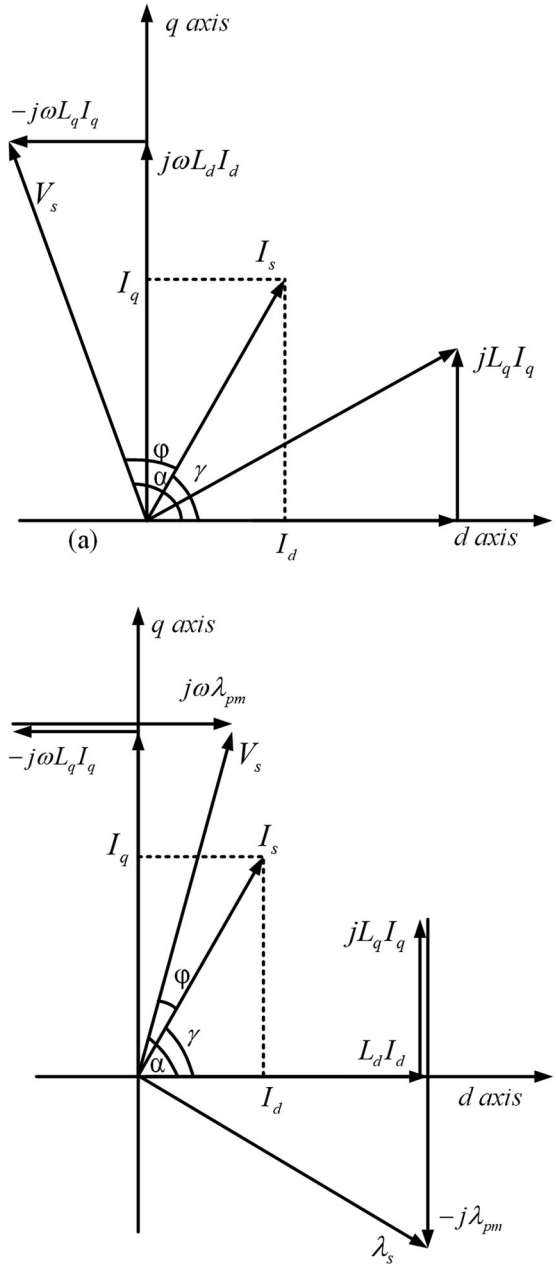

FIGURE 3. Vector diagram of (a) Synchronous reluctance machine (b) PM assisted synchronous reluctance machine.

plotted against each machine type in Figure 2. The surface-mounted PM machine (Figure 2(a)) has the lowest saliency of almost unity ($L_d = L_q$). On the other hand, SynRM (Figure 2(f)) exhibits high saliency due to its grain-oriented anisotropy and hybrid flux guides. The saliency of SynRM must be as high as practically possible to attain a high-performance machine [8]. Although PMSynRM is not included in Figure 2, its saliency ratio is higher than that of SynRM. The other types of PM machines lie in between the two due to the magnetic flux linkage rather than the saliency (Figure 2(a–e)).

The phasor diagram of SynRM in a rotating reference frame is shown in Figure 3(a) [5]. The flux-linkage (λ_s) is developed only by the stator currents i_q and i_d in SynRM. As it can be seen, the power factor $\cos(\varphi)$ is considerably low in this type of machine resulting in poor power factor. The primary design issues are the rotor core saturation and cross-coupling impact in the air-gap. These two factors can only be reduced to a certain level in a practical machine, but can't be eliminated. Another design technique can also be used to optimize the performance, i.e. adding PMs in the barriers so that an additional torque component can be introduced to increase the performance of the machine without making changes to the dimensions [7, 16, 28].

The two torque components of PMSynRM are specified in Eq. (4). The first term is developed due to added PM flux-linkage and is limited by the volume, placement and quality of PM. The second term is called reluctance torque due to the anisotropy of the material. Figure 3(b) shows a vector diagram of PMSynRM. As it can be seen, the angle between current and voltage vector (φ) is reduced due to the added PMs. Moreover, the space vector of flux linkage is changed to increase the torque angle. Although the current i_d and i_q is not changed, the resultant flux linkage is increased. Thus, the PMs should be placed in such a way that it can introduce magnetic flux toward negative Q – axis to reduce flux-linkage in the direction as well as saturating tangential ribs.

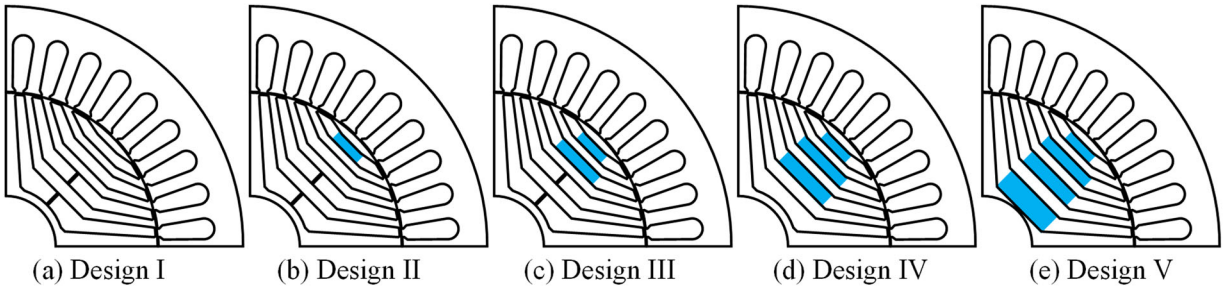

FIGURE 4. The simulated designs (a) Base design (I: SynRM), and the PMSynRMs (b) Design II (c) Design III, (d) Design IV and (e) Design V.

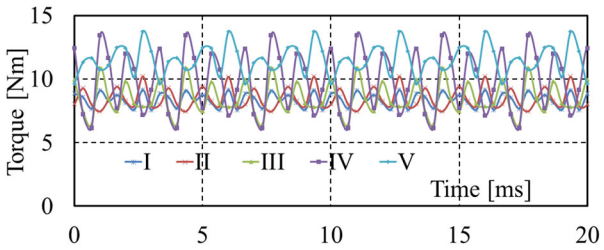

FIGURE 5. Torque behavior as a function of time for the designs shown in Figure 4 for non-skewed models.

The angle of the current vector (γ) is not significantly affected due to the added PM as can be seen in Figure 3(b). However, due to the added PM flux linkage (λ_m), the voltage vector is moved into the first quadrature. The phasor angle φ between the current and voltage vector is reduced. Thus, the added magnets should increase the power factor of the machine. The PM flux linkage is not only impacting the Q axis flux but the residual flux in the D – axis enhances the machine performance as seen from PMSynRM's vector diagram (Figure 3b).

PM Volume Analysis

Although permanent magnets are positioned along the Q – axis in recent PMSynRM the other topologies have also been suggested such as adding PMs to improve D – axis flux by placing PMs in the intermediate axis [4, 12, 17, 18]. The PM, along the Q axis, makes the analysis somewhat linear which simplifies the design. Nevertheless, the impact of PM flux linkage, various PM arrangements are studied. In this section, PMs are added along the Q – axis, as shown in Figure 4 in four different volumes and the next section deals with permanent magnet optimization. In addition, SynRM is generally limited by its drive rating, which is the maximum electrical loading. Thus, its flux linkage is also limited by loading of the machine at constant torque region and by the voltage at high-speed region.

The torque is proportionate to flux, current, and sine angle of the two, which is equivalent to magnetic and electrical loadings of the machine. Figure 4(a) is considered as the base design (SynRM) with simplified flux barrier, and the other four designs have PMs in the barriers in various quantities as shown in Figure 4(b–e). The PMs are added in barrier linear section along the Q –axis in these designs. The quantity of PM in design II is significantly smaller than that of design III and so forth. The radial webs of designs IV and V is removed to accommodate PMs. Therefore, its saliency ratio will be slightly better than the other two designs. The torques as a function of instantaneous time of all models are shown in Figure 5. The simulation is performed with fine time steps to improve the resolution of torque variation at maximum torque per ampere for each design (MTPA)

The above five designs utilize the same SynRM models except for the ones with PMs that do not have radial ribs. As can be seen, the first barrier of design-V is slightly modified to accommodate PM. It results in a tinnier steel segment between the first barrier and shaft. It is highly susceptible to saturation due to D axis flux. However, the intensity of the flux in the segment is very low as it is located close to the shaft, which is discussed later in the paper.

Reluctance and PM Flux Torque

As the base design is unchanged throughout the investigation, the reluctance torque is constant and equivalent to the SynRM torque. The quantity of added PMs is different in each design. Thus, the saturation level in the tangential ribs is also different in each design. The instantaneous torques of PMSynRMs are higher than the base design as shown in Figure 5 due to added PMs. The torques of designs II to V have 1.5%, 4.8%, 17% and 38.9% PM torques respectively. The quantities of PM in design IV and V are significantly higher than that of the design II and III. Furthermore, more

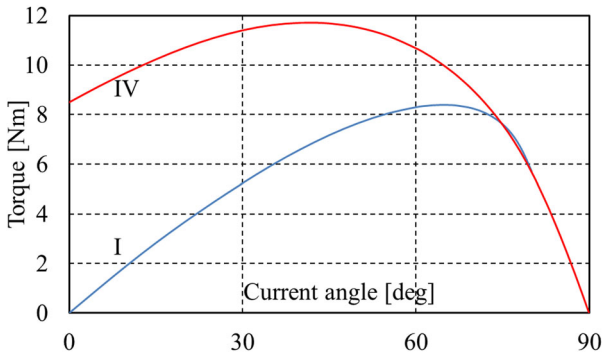

FIGURE 6. Torque of designs I and V as a function of the current angle.

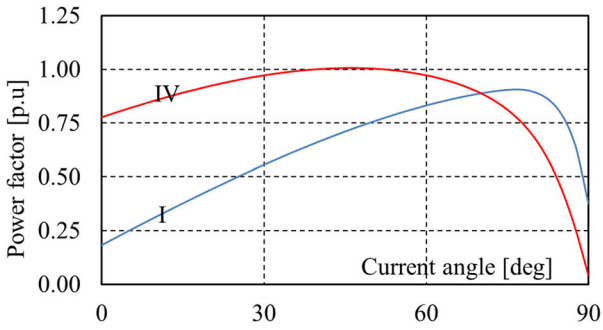

FIGURE 7. Power factor of designs I and V as a function of the current angle.

layers of PMs saturate the webs better than one or two PMs as in the case of design II and III. Although the torque is increased with more PM in each machine, the torque ripples are also increased to a level the machine cannot be used as can be seen in Figure 5.

The designs I and V are further analyzed to understand the characteristics of the SynRM and PMSynRM. In general, SynRM is controlled by the current. Thus, its true characteristics in real-time operation can be revealed by studying with respect to current. As the PMSynRM is not vastly different from SynRM and shares the same characteristics in terms of torque and power factor, this machine should also be controlled by current regulated inverter. Thus, PMSynRM should also be investigated for current. Torques of the two designs as a function of the current angle is plotted in Figure 6. As the reluctance torque is not changed much between the two designs, it is easy to estimate the torque developed by added PMs in design-V compared with its SynRM.

The maximum torque (MTPA) is obtained at a torque angle of around 45° for this machine where are SynRM's maximum torque lies at a quite higher angle (around 65°). In theory, the MTPA of SynRM should be around 45°, but due to the saturation and cross-saturation, it is drifted to a higher angle. The higher the saturation, the higher the MTPA angle is in SynRM. Whereas PMSynRM is quite different. It is a hybrid torque machine with the reluctance and PM torques.

The direct axis current (i_d) is used for magnetizing the core whereas quadrature axis current (i_q) is used for loading as can be seen in the phasor diagrams. The core of this machine is magnetized even before the current is introduced. Accordingly, the MTPA angle is lower than an equivalent SynRM as can be seen in Figure 6. The angle changes with the PM flux linkage.

The Power Factor of SynRM and PMSynRM

The power factor angle of a SynRM is larger than the MTPA angle as shown in Figure 7. Therefore, SynRM can be controlled for either torque or power factor based on the field requirement. In general, SynRM's power factor angle is 10° more than that of the torque angle. The maximum power factor changes ± 5° with changing currents.

Maximum power factor angle of a PMSynRM is considerably lower than that of SynRM. The difference depends on the strength of the added PM flux. The SynRM does not generate reluctance torque at 0°. On the other hand, PMSynRM's residual torque (magnetic torque) makes this machine to operate at a lower speed with better torque density. The above simulation is only performed to investigate the exact characteristics of PMSynRM with respect to varying PM flux linkages. The design V, although shows high torque density and almost unity power factor, possess high initial torque due to the high-grade neodymium magnets. In other words, the rotor is locked itself with stator due to the high magnetic flux at the initial position, and high inertia is required to start the machine. In addition, torque ripples and cogging torque of this design is very high.

Torque Ripples Improvement

The torque ripples are the variation of torque as a function of time during regular operation and defined by Eq. (5). SynRM is renowned for high torque ripples due to its magnetic path along airgap. A machine with high torque ripples, especially in high-speed applications is rather unacceptable. Although this study does not focus on torque ripples optimization, the PMs can be used to improve the ripple effects in SynRM [6, 10].

$$T_{ripple} = \frac{T_{max} - T_{min}}{T_{avg}} = \frac{\Delta T_{pp}}{T_{avg}} \times 100 \quad (5)$$

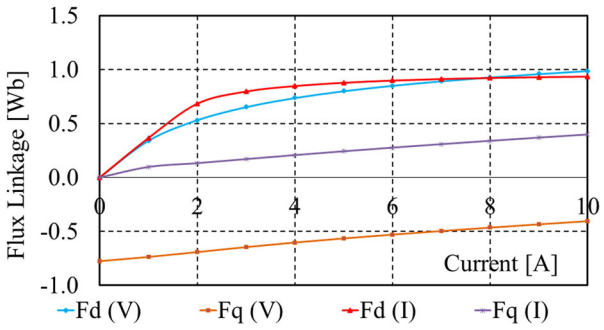

FIGURE 8. Flux linkage of design I and V as a function of current angle and supply currents.

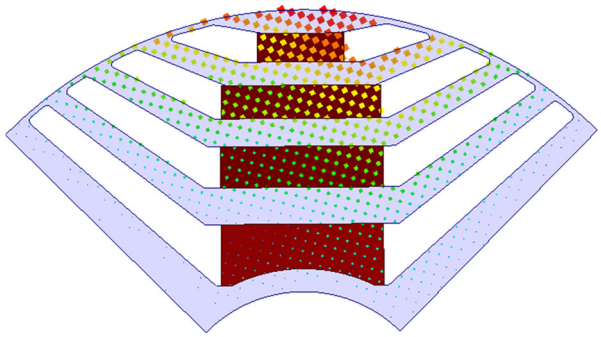

FIGURE 9. Flux intensity across Design V rotor.

The PM, in design II, equalizes the reluctance and reduce flux fluctuation due to PMs being closer to the circumference. However, further addition of PMs creates layers of flux waves through segments into the air gap, as a result, ΔL_{dq} is increased, resulting in high torque ripples. The torque ripples are increases with added PMs, as can be seen in Figure 5. The optimization of torque ripples, in SynRM, is explicitly studied and reported in [9]. In order to optimize the torque ripple effect in this type of machine, optimization of PM quantity and location on the rotor space is vital. The location of the PM and strength of the flux must be selected in such a way the ΔL_{dq} is low to reduce ripples. Thus, an automated optimization process that can optimize SynRM and PM together must be utilized rather than optimizing the quantity of PMs in a good SynRM.

PM Flux and Demagnetization in the Airgap

PM flux linkage of design I and V is plotted as a function of i_s in Figure 8. F_d of SynRM affected by saturation at around half of its rated current then it does not significantly change whereas the F_d of PMSynRM experiences saturation even before SynRM. On the other hand, F_q of SynRM is quite low and experiences saturation at one-fourth of the rated current of the machine. It is due to the thin tangential ribs. The saturation ensures that further flux via the ribs is restricted. However, as can be seen in, it slightly increases even after the saturation due to increasing current. Thus, the saliency of the machine is also affected by increasing current. It is the reason for changing MTPA and power factor angles with respect to the current angle.

It is apparent that the added PMs in the negative Q – axis saturate the tangential ribs and minimizes flux in this direction resulting in increased saliency ratio of the machine. On the other hand, the saturation of F_q of PMSynRM is not visible in the figure as the added PMs flux saturates the ribs even before the current is applied. It introduces negative flux in the Q – axis. A significant amount of current is needed to overcome this negative flux during operation. The PMs along the circumference of the rotor experience high magnetic stress compared with the PMs closer to the center, as shown in Figure 9. Also, it is the high impact region for PMs. The Q – axis current i_q is the main source of magnetic stress on the PMs. Therefore, it is essential to optimize the size of the PMs along the circumference with its location to improve machine performance as well as to reduce demagnetization.

PM Optimization

So far, PMSynRM is designed using a good SynRM. This study, for the first time proposes a novel topology to optimize both SynRM and PMs as a whole object in single optimization so that the full potential of PMSynRM can be revealed. A primitive design technique is used for this optimization. PMs are modeled on the SynRM rotor using subtraction method so that when the dimensions of flux barriers are changed by optimizer, the dimensions of PMs adopt to the new dimensions of flux barriers. The method is explained in two sections. The first one is SynRM parameterization (Figure 10a) and the second one is PM parameterization (Figure 10(b)) for the optimization.

This study primarily focuses on four barrier–design. However, the below topology can also be applied to any number of barriers by merely eliminating one barrier out from the design or adding to the design shown in Figure 10(a). It shows a parameterized half pole of a four-pole rotor with optimization variables. In order to enhance the optimization process and minimize the optimization time, variables should be minimized as much as possible. Although there may be numerous ways to prepare and interconnect the variables, this study follows the below pattern based numerous

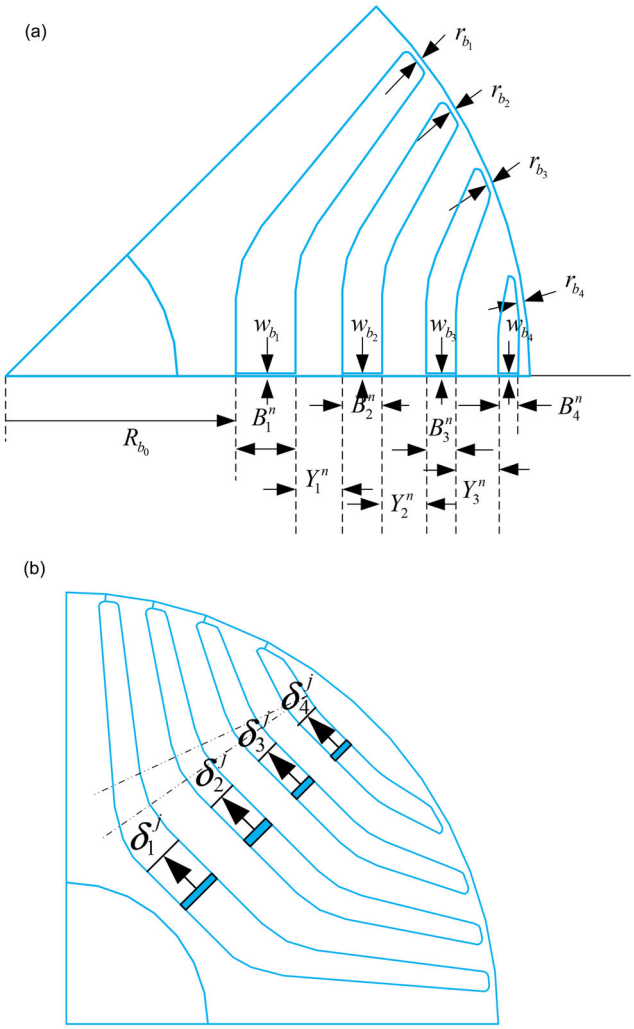

FIGURE 10. (a) SynRM optimization topology (b) PMs optimization topology.

optimization results. The pattern has been developed based on numerous optimization analysis.

The associations in Eq. (6)–(9) relate the lengths between each barrier to the center. Where$x$ is a constant. The topology can be simply changed by altering either or both of the two constants. By doing this, optimization inputs correspond to the location of barriers are minimized from four variables to a single variable, which is r. The design is shown with radial webs as this method can also be used for SynRM optimization. The webs can be eliminated by simply assigning 0 mm as in Eq. (10). As the impact of ribs is already known, it is selected as constant for the entire optimization [8, 27]. The optimizer is given higher freedom in searching optimum design by assigning individual variables for each barrier thickness (B_1^n, B_2^n, B_3^n and B_4^n). The barrier thickness variables are selected in such a way that adjacent barriers should not overlap.

$$R_{b_0} = R_{first} + r \tag{6}$$

$$R_{b_1} = R_{first} + (x+2) + \frac{2}{3}r \tag{7}$$

$$R_{b_2} = R_{first} + (x+2) + \left(\frac{2x}{3}+2\right) + 2r \tag{8}$$

$$R_{b_3} = R_{first} + (x+2) + \left(\frac{2x}{3}+2\right) + \left(\frac{x}{3}+3\right) + \frac{5}{2}r \tag{9}$$

$$\begin{aligned} r_{b_1} = r_{b_2} = r_{b_3} = r_{b_4} = 0.50\ mm \\ w_{b_1} = w_{b_2} = w_{b_3} = w_{b_4} = 0.0\ mm \end{aligned} \tag{10}$$

It minimizes the number of input variables to seven. The SynRM rotor design can be simply changed from one design to another by altering a single or multivariable during optimization. PM optimization is prepared as shown in Figure 10(b). The total number of optimization variables selected for optimization is four (δ_1^j, δ_2^j, δ_3^j and δ_4^j). The PMs are modeled using the primitive method with mirrored moving edges. Hence, if any of the variables are changed by the optimizer, the PM width change in both sides in a symmetrical arrangement. The maximum width of each PM is limited only by the length of the straight section of the respective barrier.

It is essential to have straight edge barriers to preserve the PM shape during automated optimization. If PM is extended into the none-straight section of a barrier during optimization, it may overlap into rotor segments consequently the optimization process may freeze. The barriers are modeled with straight edges in the D axis direction to ensure that the automated process does not cause any issues. Thus, the length of each PMs is limited by the flux barrier shape. It is a limitation imposed by the FEM program but not the design itself. As shown in Figure 10, the length of each PM varied from almost 0 mm (PM non-existing) to the end of the straight edge of the particular barrier. The rotor is an optimized version for SynRM. Therefore, optimization of the barrier shape is unnecessary.

The SynRM topology and PM optimization topology are combined to investigate the PMSynRM optimization with four hyperbolic barriers but without radial webs. By combining the two topologies, a design is developed to have a high degree of freedom in changing rotor and PM dimensions (optimization parameters) concurrently during optimization. As a result, eleven optimization variables are selected for multi-objective optimization. In this topology, when SynRM design parameters are altered during automated optimization, the PMs dimensions are altered concurrently in such a way that can fit into the new barriers of the new SynRM. It is achieved by designing a PM larger

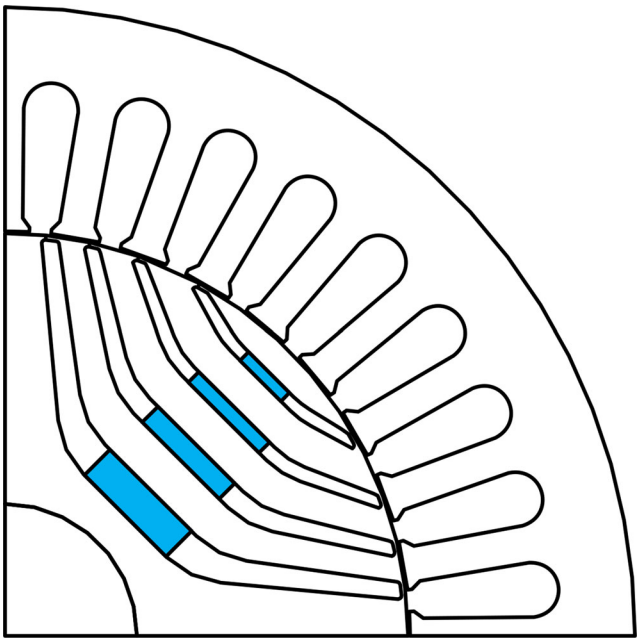

FIGURE 11. Optimized PMSynRM.

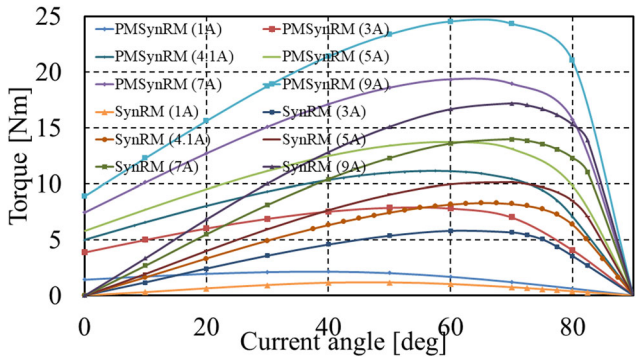

FIGURE 12. Torques of optimized PMSynRM and SynRM as a function of current and current angle.

than that of the barrier and subtracting it from the rotor design. The subtraction is stored in the design memory.

Hence, when the SynRM design parameters are altered, the subtraction automatically adjusts the PM dimensions to suit the new parameters. As the initial PM is larger than that of the barrier, it can still fit in. Thus, initial PM design is the critical element in this topology. Single–objective optimization (SOO) is a good tool if the problem has only a single target or problem's objectives are interconnected. Especially, it is a good tool to fine-tune the final product. In this case of SynRM, objectives are independent of each other such as torque and power factor. Therefore, the multi-objective optimization (MOO) algorithm must be utilized for SynRM and PMSynRM so that more than one parameter can be optimized concurrently. The optimization targets are defined by (12) where three performance parameters are defined with the same weights. The rated torque (T) is set greater than 11.5 NM and power factor is set greater than 0.92. On the other hand, the torque ripples is set less than 0.5 NM.

$$T>11.5\ Nm\ \&pf>0.92\ \ \&\ \ Torque\ ripple<0.5\ Nm \quad (12)$$

The domains of the optimization variables (r, δ_n^j *and* $R_{b_n}(n=\{1,2,3,4\})$ are cautiously selected. Besides, the intention is to have a typical shape such as rectangle PMs to minimize the cost of manufacturing. The PMs' variables are selected in such a way PM nonexistence can be depicted if the optimizer is looking for such a scenario as shown in the above Figure 10(b).

Optimized Design

The optimization is performed using a highly advanced generic algorithm for multi variables. There are numerous optimum designs perceived with near targets. However, the determining factor of all was the torque ripples whose target is difficult to achieve without alternate ripple reduction topology in this case. However, all other parameters are well and truly attained. Thus, the final design is selected based on torque ripples, and it is shown in Figure 11. The optimization targets are quite high compared with its SynRM performance discussed in the above sections. The optimizer finds almost full width of the PMs While minimizing the thickness of both PMs and barriers. In this way, PM quantities are also minimized.

Optimized Torque

The torques of the optimized PMSynRM and SynRM are plotted as a function of the current angle and terminal current in Figure 12. As can be seen, the MTPA characteristics of the two machines are relatively different. Both machines have lower MTPA angle for lower current, as the current increases, the MTPA trajectories move toward higher angle due to the saturation.

The average (rated) torque of SynRM is 8.3 NM and PMSynRM is 11.15 NM, which is almost 34% more torque (PM flux torque) compared with its SynRM at rated current. Notably, the high torque is achieved at relatively lower current angle, 10 degrees lower than SynRM. Torque ripples of both machines (instantaneous torques) are plotted over a period of 40 ms in Figure 13 where it is evident that the optimized design has quite low torque ripples compared to the design used above section.

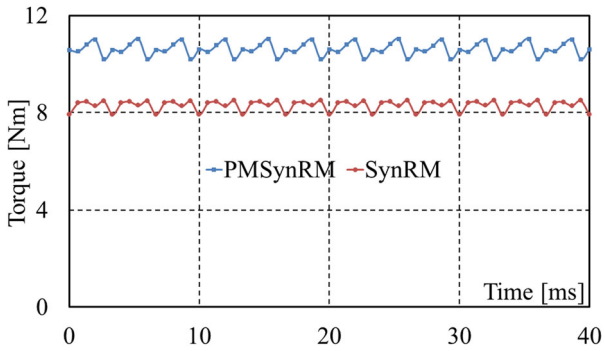

FIGURE 13. Instantaneous torques of PMSynRM and SynRM.

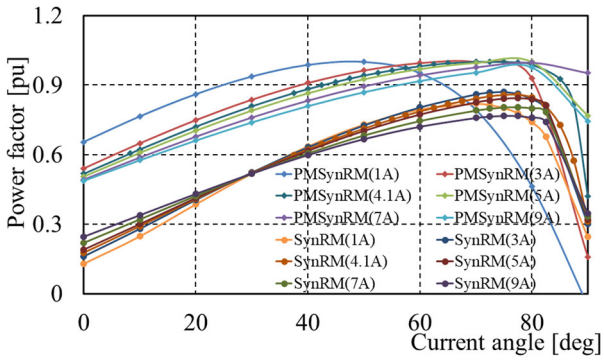

FIGURE 14. Power factor of optimized PMSynRM and SynRM as a function of the current and current angle.

Although the torque ripples target of optimization is 0.5 Nm, as discussed earlier, it is quite hard to achieve without compromising performance of the machine. The PMSynRM has torque ripples of 1.02 Nm whereas the SynRM has 0.61 Nm, which are 9.2% and 7.3% of their average torque respectively. It is well within an acceptable limit even for high-speed application.

Optimized Power Factor

The optimization target of power factor is 0.92, which is set for the PMSynRM. The optimization is performed at MTPA angle, which is lower than that of the maximum power factor current angle. At MTPA current angle, achieving this power factor is quite challenging without high-grade neodymium permanent magnets as discussed above. The optimized machines are further simulated for power factor in the first quadrant for varying currents between 1 A and 9 A, and the results are shown in Figure 14. The optimized PMSynRM shows that the maximum power factor can be almost unity at maximum power factor angle, although it is not the characteristic angle of the machine. At MTPA angle, the PMSynRM has a power factor of 0.92, and the SynRM has 0.82, which is 12% higher due to the added magnets.

The power factors of both machines seem that both can be operated with high power factor if the inverter is designed for two operational points MTPA and maximum power factor per ampere. Alternatively, the machines can be operated at a high power factor region by increasing the i_q (load current). Generally, optimum power factor of these machines lies outside the MTPA region.

PM has been proposed for SynRM to improve its performances. Although, the PMs can improve performances such as torque and power factor without a doubt, merely adding them can cause significant issues on the machine as discussed earlier. It must be optimized for efficient and smooth operation. The investigation proves that optimizing PMSynRM as a whole single object can significantly improve the performances while reducing ripples without additional arrangement such as skewing.

3. CONCLUSION

This paper investigates PMSynRM analytically and using finite element method. The first section of the study focuses on revealing the machine characteristics of the machine. It simulates PMSynRMs of various quantities of PM. The investigation has shown that adding PMs in the negative Q axis improves machine performance, such as torque and power factor. However, it introduces high cogging torque and torque ripples. The second section of the paper investigate a novel optimization method to optimize PMSynRM as a whole single object. The method utilizes primitive technique to subtract models in such a way the dimensions of the PM can adopt to the constantly changing flux barrier dimensions during optimization. PMSynRM is optimized using a generic multi-objective algorithm so that large number of optimization variables and multi optimization targets can be included in the optimization process. Optimization of just PMs using a good SynRM can't foresee the other combinations. This method ensures that the optimizer search through and consider all possible combinations and yield the best design. The optimization results from this investigation prove that optimizing PMSynRM machine as a single object can yield better performance.

REFERENCES

[1] T. Mohanarajah, J. Rizk, M. Nagrial and A. Hellany, "Finite element analysis and design methodology for high-efficiency synchronous reluctance motors," *Electric Power Components Syst.*, vol. 46, no. 13, pp. 1478–1493, 2018. DOI: 10.1080/15325008.2018.1489436.

[2] S. Ooi, S. Morimoto, M. Sanada and Y. Inoue, "Performance evaluation of a high-power-density PMASynRM with ferrite magnets," *IEEE Trans. Ind. Applicat.*, vol. 49, no. 3, pp. 1308–1315, 2013. DOI: 10.1109/TIA.2013.2253293.

[3] P. Niazi and H. A. Toliyat, "Online parameter estimation of permanent-magnet assisted synchronous reluctance motor," *IEEE Trans. Ind. Applica.t*, vol. 43, no. 2, pp. 609–615, 2007. DOI: 10.1109/TIA.2006.890021.

[4] P. Guglielmi, B. Boazzo, E. Armando, G. Pellegrino and A. Vagati, "Permanent-magnet minimization in PM-assisted synchronous reluctance motors for wide speed range," *IEEE Trans. Ind. Applicat.*, vol. 49, no. 1, pp. 31–41, 2013. DOI: 10.1109/TIA.2012.2229372.

[5] N. Bianchi, E. Fornasiero and W. Soong, "Selection of PM flux linkage for maximum low-speed torque rating in a PM-assisted synchronous reluctance machine," *IEEE Trans. Ind. Applicat.*, vol. 51, no. 5, pp. 3600–3608, 2015. DOI: 10.1109/TIA.2015.2416236.

[6] N. Bianchi, S. Bolognani, D. Bon and M. D. Pre, "Rotor flux-barrier design for torque ripple reduction in synchronous reluctance and PM-assisted synchronous reluctance motors," *IEEE Trans. Ind. Applicat.*, vol. 45, no. 3, pp. 921–928, May-June 2009. DOI: 10.1109/TIA.2009.2018960.

[7] E. Armando, P. Guglielmi, G. Pellegrino, M. Pastorelli and A. Vagati, "Accurate modeling and performance analysis of IPM-PMASR motors," *IEEE Trans. Ind. Applicat.*, vol. 45, no. 1, pp. 123–130, 2009. DOI: 10.1109/TIA.2008.2009493.

[8] T. Mohanarajah, J. Rizk, M. Nagrial, and A. Hellany, "Design of synchronous reluctance motors with improved power factor," 11th IEEE International Conference on Compatibility, Power Electronics and Power Engineering, in *(*CPE-POWERENG), 4-6 April 2017, 2017, pp. 340–345. DOI: 10.1109/CPE.2017.7915194.[10.1109/CPE.2017.7915194]

[9] T. Mohanarajah, J. Rizk, A. Hellany, M. Nagrial, and A. Klyavlin, "Torque ripple improvement in synchronous reluctance machines," 2nd International Conference on Electrical Engineering (EECon), 2018, 28-28 Sept. pp. 44–50. DOI: 10.1109/EECon.2018.8541021.[10.1109/EECon.2018.8541021]

[10] S. Stipetic, D. Zarko and M. Kovacic, "Optimised design of permanent magnet assisted synchronous reluctance motor series using combined analytical & finite element analysis based approach," *IET Electric Power Applicat.*, vol. 10, no. 5, pp. 330–338, 2016. DOI: 10.1049/iet-epa.2015.0245.

[11] P. Niazi, H. A. Toliyat, D. H. Cheong and J. C. Kim, "A low-cost and efficient permanent-magnet-assisted synchronous reluctance motor drive," *IEEE Trans. Ind. Applicat.*, vol. 43, no. 2, pp. 542–550, 2007. DOI: 10.1109/TIA.2006.890033.

[12] H. Huang, Y. Hu, Y. Xiao and H. Lyu, "Research of parameters and antidemagnetization of rare-earth-less permanent magnet-assisted synchronous reluctance motor," *IEEE Trans. Magn.*, vol. 51, no. 11, pp. 1–4, 2015. DOI: 10.1109/TMAG.2015.2445934.

[13] N. Bianchi, M. Degano and E. Fornasiero, "Sensitivity analysis of torque ripple reduction of synchronous reluctance and interior PM motors," *IEEE Trans. Ind. Applicat.*, vol. 51, no. 1, pp. 187–195, 2015. DOI: 10.1109/TIA.2014.2327143.

[14] M. Barcaro, T. Pradella and I. Furlan, "Low-torque ripple design of a ferrite-assisted synchronous reluctance motor," *IET Electric Power Applicat.*, vol. 10, no. 5, pp. 319–329, 2016. DOI: 10.1049/iet-epa.2015.0248.

[15] M. Barcaro, N. Bianchi and F. Magnussen, "Permanent-magnet optimization in permanent-magnet-assisted synchronous reluctance motor for a wide constant-power speed range," *IEEE Trans. Ind. Electron*, vol. 59, no. 6, pp. 2495–2502, 2012. DOI: 10.1109/TIE.2011.2167731.

[16] T. Mohanarajah, J. Rizk, M. Nagrial, and and A. Hellany, "Permanent magnet optimization in PM assisted synchronous reluctance machines," in IEEE 27th International Symposium on Industrial Electronics (ISIE), 13-15 June, 2018, pp. 1347–1351. DOI: 10.1109/ISIE.2018.8433589.

[17] N. Bianchi, E. Fornasiero, M. Ferrari and M. Castiello, "Experimental comparison of PM-assisted synchronous reluctance motors," *IEEE Trans. Ind. Applicat.*, vol. 52, no. 1, pp. 163–171, 2016. DOI: 10.1109/TIA.2015.2466623.

[18] N. Bianchi, S. Bolognani, E. Carraro, M. Castiello and E. Fornasiero, "Electric vehicle traction based on synchronous reluctance motors," *IEEE Trans. Ind. Applicat.*, vol. 52, no. 6, pp. 4762–4769, 2016. DOI: 10.1109/TIA.2016.2599850.

[19] D. Prieto, P. Dessante, J. C. Vannier, B. Dagusé, X. Jannot and J. Saint-Michel, "Multi-physic analytical model for a saturated permanent magnet assisted synchronous reluctance motor," *IET Electric Power Applicat.*, vol. 10, no. 5, pp. 356–367, May 2016. DOI: 10.1049/iet-epa.2015.0199.

[20] F. Xing, W. Zhao and B. Kwon, "Design and optimisation of a novel asymmetric rotor structure for a permanent magnet-assisted synchronous reluctance machine," *IET Electric Power Applicat.*, vol. 13, no. 5, pp. 573–580, 2019. DOI: 10.1049/iet-epa.2018.0184.

[21] S. S. R. Bonthu, M. T. B. Tarek and S. Choi, "Optimal torque ripple reduction technique for outer rotor permanent magnet synchronous reluctance motors," *IEEE Trans. Energy Convers.*, vol. 33, no. 3, pp. 1184–1192, Sept. 2018. DOI: 10.1109/TEC.2017.2781259.

[22] Y. Wang, G. Bacco and N. Bianchi, "Geometry analysis and optimization of permanent magnet-assisted reluctance motors," *IEEE Trans. Ind. Applicat.*, vol. 53, no. 5, pp. 4338–4347, 2017. DOI: 10.1109/TIA.2017.2702111.

[23] K. Yamazaki, S. Tamiya, K. Utsuno, K. Shima, T. Fukami and M. Sato, "Rotor Shape optimization for output maximization of permanent-magnet-assisted synchronous machines," *IEEE Trans. Ind. Applicat.*, vol. 51, no. 4, pp. 3077–3085, July-Aug. 2015. DOI: 10.1109/TIA.2015.2407852.

[24] R. Vartanian and H. A. Toliyat, "Design and comparison of an optimized permanent magnet-assisted synchronous reluctance motor (PMa-SynRM) with an induction motor with identical NEMA Frame stators," IEEE Electric Ship Technologies Symposium, 2009, 20-22 April pp. 107–112. DOI: 10.1109/ESTS.2009.4906501.

[25] H. Murakami, Y. Honda, Y. Sadanaga, Y. Ikkai, S. Morimoto, and Y. Takeda, "Optimum design of highly efficient magnet assisted reluctance motor," Conference Record of the IEEE Industry Applications Conference. 36th IAS Annual Meeting (Cat. No.01CH37248), 30 Sept.-4 Oct, 2001, vol. 4, pp. 2296–2301. DOI: 10.1109/IAS.2001.955944.

[26] Z. Zhengming and E. A. Ahmed, "Optimization of added permanent magnet amount in synchronous reluctance machines for high performance," *Tsinghua Sci. Technol.*, vol. 3, no. 3, pp. 1137–1142, 1998.

[27] T. Mohanarajah, J. Rizk, M. Nagrial, and A. Hellany, "Analysis and design of high-performance synchronous reluctance machine," IEEE 12th International Conference on Compatibility, Power Electronics and Power Engineering, 2018, in *(*CPE-POWERENG-2018), 10-12 April 2018, pp. 1–6. DOI: 10.1109/CPE.2018.8372490.

[28] S. Morimoto, M. Sanada and Y. Takeda, "Performance of PM-assisted synchronous reluctance motor for high-efficiency and wide constant-power operation," *IEEE Trans. Ind. Applicat.*, vol. 37, no. 5, pp. 1234–1240, 2001. DOI: 10.1109/28.952497.

BIOGRAPHIES

Thushanthan Mohanarajah received his B.E. in Mechatronics from University of Technology, Sydney and B.E. in Electrical Engineering from University of Western Sydney University and currently has been working toward his PhD at Western Sydney University. He is a professional engineer and member of Engineers Australia. He has published numerous papers in international conferences. His research interest is primarily in the area of electrical machine design, drive design, and optimization on machine performance.

Mahmood Nagrial obtained his PhD from the University of Leeds, UK. He has been Head of Electrical & Computer Engineering and Chair, School of Mechatronic, Computer & Electrical Engineering at Western Sydney University. He has also been responsible for initiating undergraduate, postgraduate courses and higher degree research programs in Electrical & Computer Engineering, Mechatronic Engineering. He has been the group leader of "Intelligent & Sustainable Electrical Systems" research group. He has supervised PhD and M.Eng. (Hons) research theses and postdoctoral fellows. Before joining Western Sydney University to start and develop engineering programs, he worked as Principal Research Scientist at CSIRO in Sydney, where he has been responsible for developing new devices using rare-earth magnets. Dr Nagrial is a Fellow of IET (UK), IE (Aust) and Fellow IE (Pak). His main expertise is in the area of a permanent magnet, variable reluctance machines & drive systems

Jamal Rizk has been a lecturer in the school of Engineering and Industrial Design, the University of Western Sydney since 1997 and a senior lecturer from 2004. He has obtained his Master of Electrical Engineering (Hons) from Kharkov Polytechnic Institute, Ukraine in 1985 and Ph. D in Electrical Engineering from the University of Western Sydney in 2001. He has acted as a reviewer for papers for many national and international conferences and journals and a member of Intelligent & Sustainable Electrical Systems (ISES). He has extensive experience in electromagnetic devices, drive systems and renewable energy. He has been involved in the design, development of permanent magnet and variable reluctance drive systems for more than 15 years. He has developed special expertise in the magnetic analysis of different types of permanent magnet machines. He has been involved in design, fabrication and testing of electrical drives. He has also developed research interests in integrated renewable energy systems.

Ali Hellany holds a BE in telecommunication, ME (Hons) in Electrical Engineering and a PhD in Electrical Engineering, from University of Western Sydney (Australia). Ali Hellany is a senior lecturer at the School of Engineering, the University of Western Sydney since 2002. Dr Hellany has published numerous papers in the Electromagnetic Compatibility, power quality, AC Interference, teaching styles and digital forensics area in journals and presented his research in many international conferences. He has extensive experience in power electronics and Ac interference and electromagnetic interference/compatibility. Ali is a member of Electromagnetic society. His main research interests are in the general area of power electronics electromagnetic compatibility and power quality.